

The high efficiency of $\text{Al}_2\text{O}_3\text{-SiO}_2\text{-CuO}$ nanocomposites as an adsorbent: synthesis and dye removal efficiency

Amene Nezam¹ · A. Saffar-Teluri^{1,2} ·
S. A. Hassanzadeh-Tabrizi¹

Received: 19 August 2015 / Accepted: 26 October 2015 / Published online: 16 November 2015
© Springer Science+Business Media Dordrecht 2015

Abstract In this study, $\text{Al}_2\text{O}_3\text{-SiO}_2$ and $\text{Al}_2\text{O}_3\text{-SiO}_2\text{-CuO}$ nanocomposites with different amounts of CuO (40, 50 and 60 %) were synthesized by the sol–gel method and characterized by thermogravimetric and differential thermal analysis, X-ray diffraction, Fourier transform infrared spectroscopy, field emission scanning electron microscopy, energy dispersive spectrometry and zeta potential analysis. The nanocomposites were applied as an adsorbent for removal of methylene blue (MB) from aqueous solution. The relation between removal percentages with variables such as adsorbent dosage (0.001, 0.003, 0.005, 0.01 and 0.02 g), adsorbent type and initial MB concentration (10, 20, 30 and 40 mg/L) was investigated, and optimized conditions were found to be 0.01 g, 50 % CuO and 10 mg/L, respectively. In this condition, the removal efficiency of MB was 98 %. The resulting zeta potential showed that the surfaces of $\text{Al}_2\text{O}_3\text{-SiO}_2\text{-CuO}$ nanocomposite and of $\text{Al}_2\text{O}_3\text{-SiO}_2$ have negative charges, at -45 and -15 mV, respectively, while that of CuO has a positive charge of approximately $+13$ mV.

Keywords Nanocomposites · Sol–gel · Adsorbent · Methylene blue

Introduction

The removal of dye compounds from industrial wastewater is one of the vital necessities for the survival of human beings, which has attracted much attention. Since these dyes are stable, toxic and resistant to biodegradation, to prevent their release into

✉ A. Saffar-Teluri
a.saffar.t@iaun.ac.ir

¹ Faculty of Material Science and Engineering, Najafabad Branch, Islamic Azad University, P. O. Box 85141-43131, Najafabad, Isfahan, Iran

² Department of Chemistry, Faculty of Science, Najafabad Branch, Islamic Azad University, P.O. Box 85141-43131, Najafabad, Isfahan, Iran

environment, they must be removed from effluents by different methods such as coagulation, flocculation, oxidation processes and membrane separation. In spite of the potential utility of these methods for removal of dyes, many of the aforementioned routes involve expensive reagents and long interaction times. Therefore, to avoid these limitations, the use of an efficient method with high removal activity and short interaction times is of prime interest. Adsorption is an interesting technique for removal of dyes from wastewater. This technique, due to prominent properties such as high efficiency, simplicity and reusability, has become one of the most promising techniques for dye removal from industrial wastewaters [1–24].

$\text{Al}_2\text{O}_3\text{--SiO}_2$ mixed oxides are important ceramic materials that, as inorganic supports, are widely used in catalytic activities [25–32]. The application of these materials as supports is due to the existence of Al–O–Si bond structures and $\text{SiO}_2\text{--Al}_2\text{O}_3$ interfaces. Also, a low thermal conductivity, low dielectric constant, robust chemical and thermal stability and oxidation resistance are the reasons for using these particular mixed oxides in industry.

The oxides of transition metals are an important class of semiconductors, which have wide different applications according to their physical and chemical properties. Among the transition metal oxides, copper oxide and its composites have potential applications in electro-oxidation of hydrazine [33], water–gas shift reactions [34], oxidation of CO [35], hydrogenation of CO_2 to methanol [36] and synthesis of diaryl ether [37].

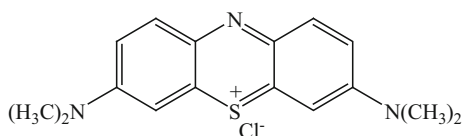
Due to the versatile properties and diverse applications of copper oxide and $\text{Al}_2\text{O}_3\text{--SiO}_2$, in this paper, $\text{Al}_2\text{O}_3\text{--SiO}_2\text{--CuO}$ nanocomposites with different amounts of CuO (40, 50 and 60 %) were synthesized by the sol–gel method and characterized by Fourier transform infrared (FT-IR) spectroscopy, simultaneous thermal analysis (STA), X-ray diffraction (XRD), field emission scanning electron microscopy (FE-SEM), energy dispersive spectrometry (EDS) and zeta potential analysis. These nanocomposites were used as an adsorbent for the removal of methylene blue (MB) from aqueous solution. MB is a typical water-soluble cationic dye and has harmful effects on living organisms in a short period of exposure (Fig. 1).

Experimental

Materials and the synthesis of nanocomposites

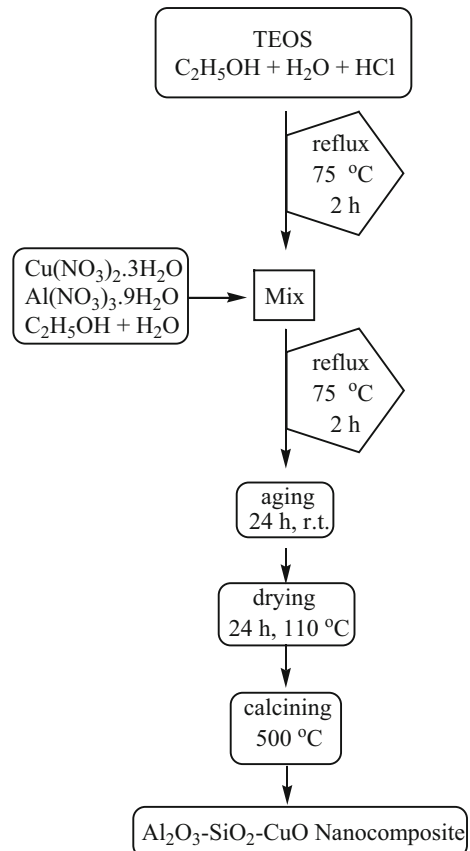
All reagents were purchased from Merck and Aldrich and used without further purification. Copper nitrate ($\text{Cu}(\text{NO}_3)_2 \cdot 3\text{H}_2\text{O}$), aluminum nitrate ($\text{Al}(\text{NO}_3)_3 \cdot 9\text{H}_2\text{O}$)

Fig. 1 Chemical structure of methylene blue



and tetraethylorthosilicate (TEOS) were used as copper, aluminum and silicon precursors, respectively. Al₂O₃-SiO₂-CuO nanocomposites with 40, 50 and 60 wt% of CuO were synthesized using the sol-gel approach according to Fig. 2. Firstly, TEOS was diluted in ethanol and water. Then, the necessary amount of HCl (37 %) was added to the mixture and refluxed in 75 °C for 2 h (TEOS:C₂H₅OH:H₂O:HCl molar ratio was 1:22:13:7.9 × 10⁻⁴). Afterward, copper nitrate (Cu(NO₃)₂·3H₂O) and aluminum nitrate (Al(NO₃)₃·9H₂O) dissolved in ethanol and water were added to the mixture and refluxed at 75 °C for another 2 h. The resulting mixture was aged at room temperature for 24 h and dried in an oven for 24 h at 110 °C. Then, they were calcined to 500 °C at a heating rate of 8 °C/min and, once 500 °C was reached, they were kept at this temperature for 5 h. The nominal content of CuO was 0, 40, 50 and 60 wt%, and the corresponding nanocomposites were denoted as Al₂O₃-SiO₂, Al₂O₃-SiO₂-40 % CuO, Al₂O₃-SiO₂-50 % CuO and Al₂O₃-SiO₂-60 % CuO, respectively. For comparison, pure CuO nanocomposites were also prepared with the same procedure. The flow chart of the nanocomposite synthesis is shown in Fig. 2.

Fig. 2 The flowchart of the preparation of Al₂O₃-SiO₂-CuO nanocomposites



Characterization

FT-IR spectroscopy was performed using a Jasco FT/IR-3600 FT-IR spectrometer. The phase and crystallinity were characterized using a Philips x'pert X-ray diffractometer with Cu-K α radiation in the 2θ range of 10–80°. Zeta potential analysis of 60 wt% nanocomposite dispersed in water was achieved using a Malvern Zetasizer Nano instrument at 25 °C. The morphologies of prepared samples were investigated FE-SEM. The weight change of composite samples was measured using a thermogravimetric analysis (TGA)/differential thermal analysis (DTA) simultaneous thermal analyzer apparatus (METTLER TGA/SDTA 851E) under a flow of dry air.

Adsorption experiments

The dye removal experiment was conducted at room temperature as batches. Typically, a stock solution (1 g/L) of MO dye was prepared in deionized water, then experimental solutions with different initial concentrations (10–40 mg/L) were obtained by successive dilutions. The required amount of Al₂O₃–SiO₂–CuO nanocomposite was added into the 10-mL dye solution and stirred for the predefined time. After that, the suspension was centrifuged and the supernatant was analyzed by ultraviolet–visible light (UV–Vis) spectroscopy to calculate the residual dye concentration. The removal of dye percentage (R) was calculated using equation:

$$R = \frac{(C_0 - C_t)}{C_0} \times 100 \quad (1)$$

where C_0 is the initial concentration and C_t is the concentration of the dye at time t .

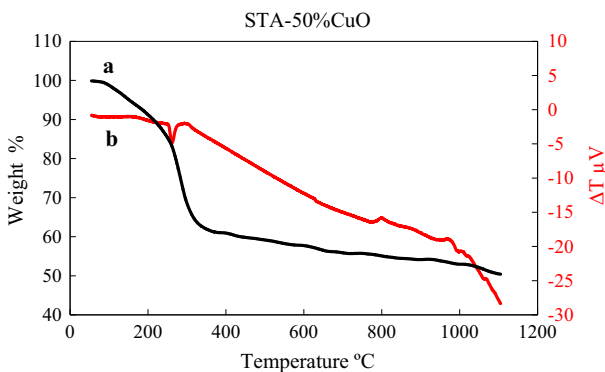


Fig. 3 TGA (a) and DTA (b) patterns of the precursor of Al₂O₃–SiO₂–50 % CuO sample

Results and discussion

Thermal analysis

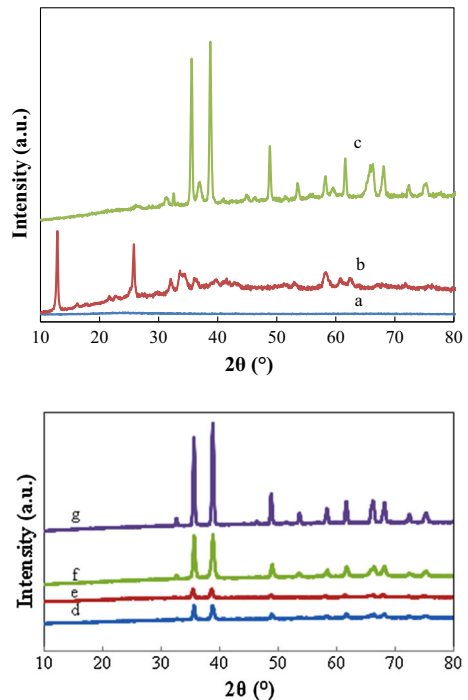
The TGA/DTA result of the Al₂O₃-SiO₂-50 % CuO precursor is shown in Fig. 3a, b.

The process of weight loss can be divided into two steps. The endothermic peak between 50 and 200 °C on DTA, accompanied by a 12 % weight loss observed in this first step on the TGA curve, is attributed to the desorption of water and solvent (that may be physical or chemical adsorption on the interparticle surface of the sample). The second peak from 200 to 400 °C with a main weight loss of about 28 %, accompanied by an endothermic peak at 370 °C, corresponds to the weight loss of dehydroxylation caused by breaking of Si-OH and Al-OH bonds and the calcination of the CuO precursor. The two exothermic peaks at 750–850 and 950–1100 °C on DTA are attributed to the formation of the crystalline phases of CuAl₂O₄ and CuAlO₂, respectively.

XRD analysis

XRD patterns of the samples prepared before and after heat treatment at 600 °C for 3 h are shown in Fig. 4a–c. According to the XRD analysis in Fig. 4a, no peak for Al₂O₃-SiO₂ is observed. This confirms that Al₂O₃-SiO₂ has an amorphous phase. For the precursor of Al₂O₃-SiO₂-50 % CuO sample before heating at 600 °C, the

Fig. 4 XRD patterns of the calcined samples at 600 °C [Al₂O₃-SiO₂ (a), the precursor of Al₂O₃-SiO₂-50 % CuO sample (b), Al₂O₃-SiO₂-50 % CuO (c)]; the calcined samples at 500 °C [Al₂O₃-SiO₂-40 % CuO (d), Al₂O₃-SiO₂-50 % CuO (e), Al₂O₃-SiO₂-60 % CuO (f) and 100 % CuO (g)]



patterns corresponding to the copper nitrate are presented as the partially hydrolyzed phase of $\text{Cu}_2(\text{OH})_3(\text{NO}_3)$. This phase is confirmed by the patterns appearing at $2\theta = 12.91^\circ, 25.83^\circ, 32.09^\circ, 33.64^\circ, 34.31^\circ, 36.14^\circ, 58.40^\circ, 60.81^\circ$ and 62.55° in Fig. 4b. The observed diffraction peaks after heating at 600°C with 2θ values of $32.5^\circ, 35.4^\circ, 38.6^\circ, 49.0^\circ, 53.4^\circ, 58.1^\circ, 61.5^\circ, 66.0^\circ, 67.9^\circ$ and 72.3° correspond to diffraction from the planes of crystalline CuO (Fig. 4c). These diffraction data are in good agreement with the Joint Committee on Powder Diffraction Standards (JCPDS) card of the monoclinic CuO structure (JCPDS 80-1268). But, in this XRD spectrum, the other diffraction peaks with 2θ values of $31.2^\circ, 37.1^\circ, 45.0^\circ, 56.0^\circ, 59.0^\circ$ and 65.5° can also be attributed to the CuAl_2O_4 phase having a perovskite crystal structure (PDF [78-1605]). Since our aim in this study is the formation of $\text{Al}_2\text{O}_3\text{-SiO}_2\text{-CuO}$ nanocomposites, we, therefore, decreased the heat treatment to 500°C . The XRD patterns of the precursor powders calcined in air at 500°C are shown in Fig. 4d–g. According to the XRD analyses, all the diffraction lines in these XRD spectra could be attributed to the CuO phase having a monoclinic structure.

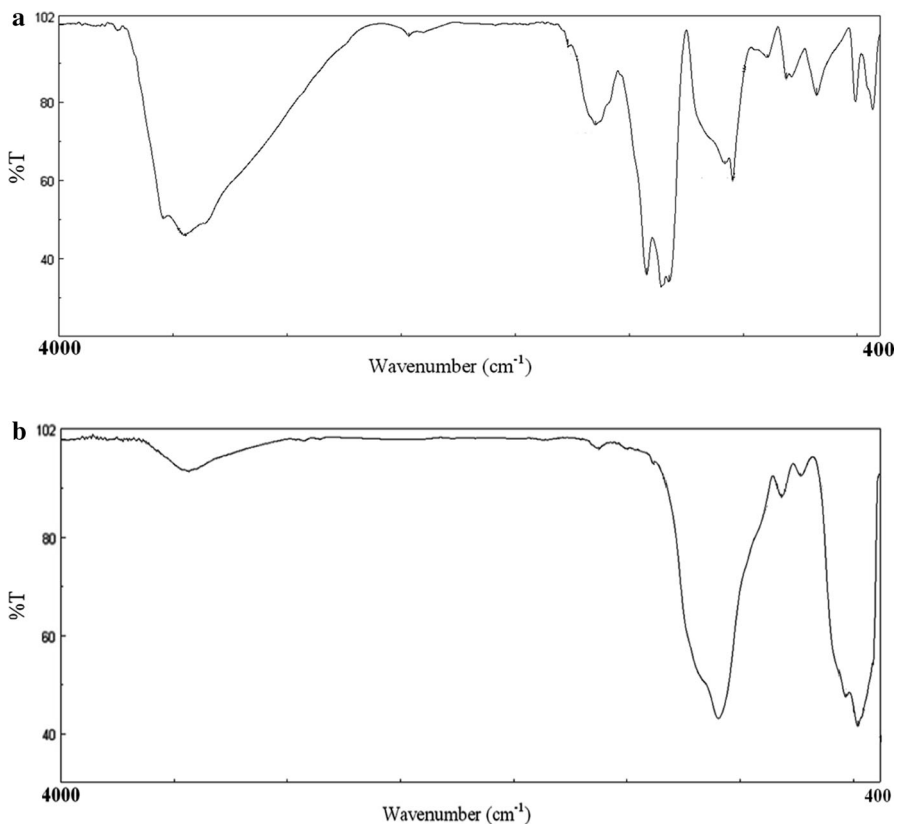


Fig. 5 FT-IR spectra of $\text{Al}_2\text{O}_3\text{-SiO}_2\text{-50 % CuO}$ sample before (a) and after (b) calcining at 500°C

FT-IR analysis

Figure 5a, b presents the FT-IR spectra of Al₂O₃-SiO₂-50 % CuO sample before (a) and after (b) calcining at 500 °C.

In Fig. 5a, the adsorption peaks at 3448 and 1649 cm⁻¹ are attributed to the stretching vibration and bending vibration of the O-H group for water, respectively. The absorption at 2465 cm⁻¹ is because of the existence of CO₂ molecules in air. The presence of nitrate ions in the sample is confirmed using a very strong band at 1354 cm⁻¹, which is due to asymmetric NO₃⁻ stretching vibration [38]. The bending absorption of a Cu-O-H bond at 678 cm⁻¹ and discussed later shows that the copper species in a dried precursor is mainly present in the form of

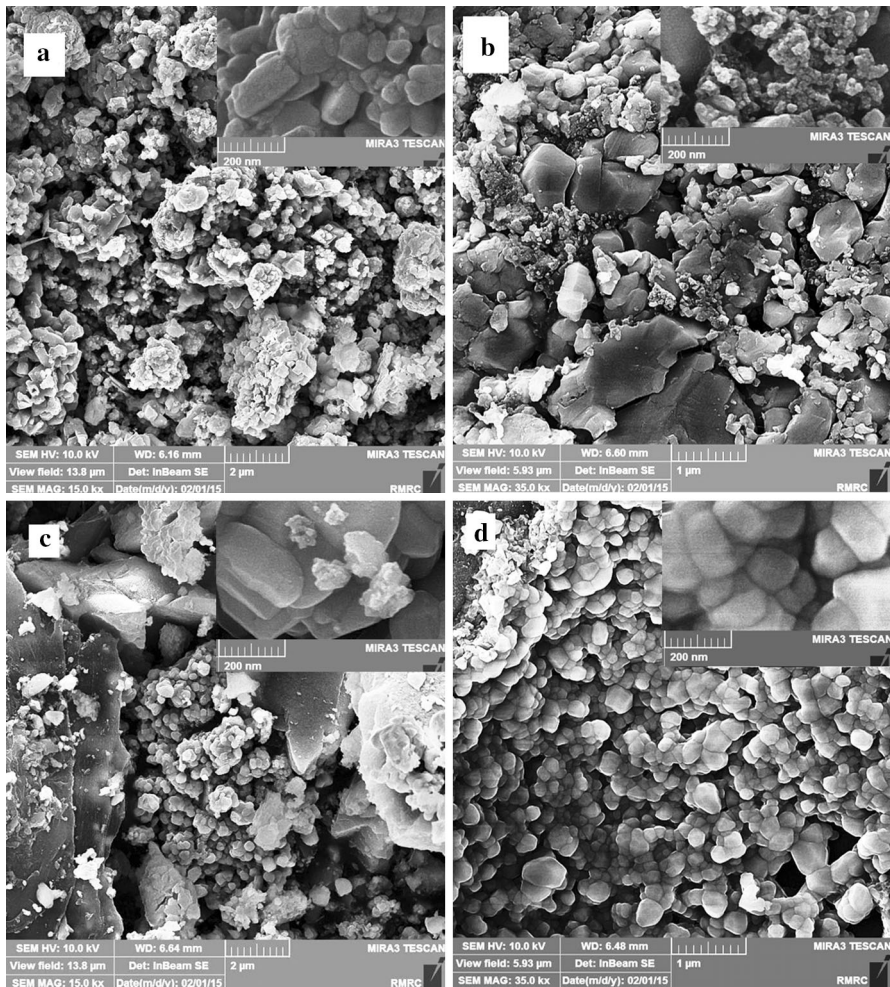


Fig. 6 FE-SEM images of the calcined samples at 500 °C (100 % CuO (a), Al₂O₃-SiO₂-40 % CuO (b), Al₂O₃-SiO₂-50 % CuO (c) and Al₂O₃-SiO₂-60 % CuO (d))

$\text{Cu}_2(\text{OH})_3\text{NO}_3$, which was confirmed by the XRD pattern. The absorption peak of Al–O stretching vibration in the range of $1000\text{--}1200\text{ cm}^{-1}$ could not be resolved due to its overlap with the absorption peak of Si–O–Si stretching vibration in the range of $1000\text{--}1200\text{ cm}^{-1}$. Also, the peaks between $420\text{ and }550\text{ cm}^{-1}$ correspond to the Al–O and Cu–O bond vibration [39–43]. The individual peaks corresponding to Cu–O bond and Al–O bond are obtained only when the sample is calcined at $500\text{ }^\circ\text{C}$. In Fig. 5b, the absorption peaks $480\text{ and }533\text{ cm}^{-1}$ are attributed to Cu–O vibration, whereas the peaks obtained at $731\text{ and }815\text{ cm}^{-1}$ indicate Al–O bond vibrations. There are also bands at $900\text{ and }1095\text{ cm}^{-1}$ due to the Al–O–Al and Si–O–Si bond stretching vibration. The stretching vibration and bending vibration of an O–H group for water appears at $3435\text{ and }1622\text{ cm}^{-1}$, respectively.

FE-SEM images of nanocomposites

Figure 6a–d shows the FE-SEM images of the samples with different compositions calcined at $500\text{ }^\circ\text{C}$. Recently, we reported that the synthesized $\text{Al}_2\text{O}_3\text{--SiO}_2$ by the sol–gel method has an amorphous and homogenous structure [44]. According to Fig. 6, the roughness of the surface in the nanocomposites can be clearly observed and it is more than that in an $\text{Al}_2\text{O}_3\text{--SiO}_2$ specimen. $\text{Al}_2\text{O}_3\text{--SiO}_2\text{--CuO}$ nanocomposite surface roughness can be attributed to (1) the insolubility of CuO in a SiO_2 matrix, (2) and the crystal growth of CuO in an $\text{Al}_2\text{O}_3\text{--SiO}_2$ matrix.

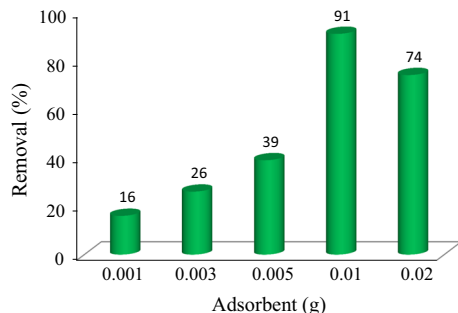
Adsorption efficiency of nanocomposites

In order to characterize the removal activity of synthesized samples, an aqueous solution of MB as an azo and cationic dye (Fig. 1) was selected and the removal activity was done with this solution. The effect of adsorbent dosage, concentration of MB and kind of adsorbent was investigated for optimizing adsorption conditions.

Influence of adsorbent dosage on the removal efficiency of MB

The effect of adsorbent dosage on removal of MB (20 mg/L) was studied with $\text{Al}_2\text{O}_3\text{--SiO}_2\text{--}50\text{ }\%$ CuO nanocomposite as the adsorbent, and the results are shown in Fig. 7. By increasing the amount of the adsorbent from 0.001 to 0.01 g , the

Fig. 7 The effect of adsorbent dosage on removal of MB



removal efficiency of MB increased from 16 to 91 %. This was due to the active sites being enhanced with an increased amount of Al₂O₃-SiO₂-50 % CuO nanocomposite. However, with a further increase in adsorbent dosage to 0.02 g, there is a decrease in the efficiency of MB removal to 74 %. Consequently, a dosage of 0.01 g was selected as the optimum value.

Influence of initial MB concentration on the removal efficiency of MB

Another important parameter that affects the adsorption of dye is the initial dye concentration of the solution. As shown in Fig. 8, the percentage of MB removal decreased from 98 to 64 % with the increase in initial MB concentration from 10 to 40 mg/L. This effect can be explained by a reduction in active sites on the adsorbent's surface, which leads to a decrease in the percentage of MB removal [45].

Influence of the kind of adsorbent on the removal efficiency of MB

Figure 9 indicates that the amount of CuO in the nanocomposites influences the adsorption efficiency of MB. The highest adsorption was obtained for the Al₂O₃-SiO₂-50 % CuO nanocomposite (98 %). The high adsorption may be due to the abundant availability of active sites on the nanocomposite's surface. By increasing the amount of the CuO to 60 %, these sites were gradually decreased; therefore, the adsorbent became less efficient.

Zeta potential

The surface charge of an adsorbent is a one of the important parameters in the adsorption process. In order to confirm the adsorption results, the structures of the nanocomposites were studied by determination of zeta potential. The surfaces of Al₂O₃-SiO₂-50 % CuO and Al₂O₃-SiO₂ have negative charges of -45 and -15 mV, respectively, while that of CuO has a positive charge about +13 mV. The high adsorption of MB using Al₂O₃-SiO₂-50 % CuO can be attributed to its more negative surface charge.

Fig. 8 The effect of initial MB concentration on the removal efficiency of MB

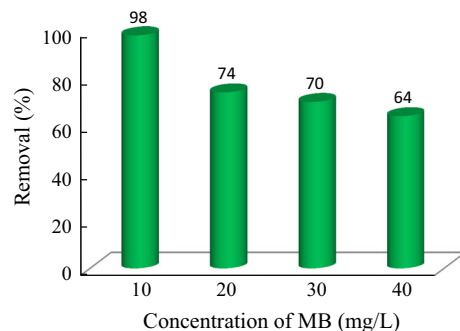
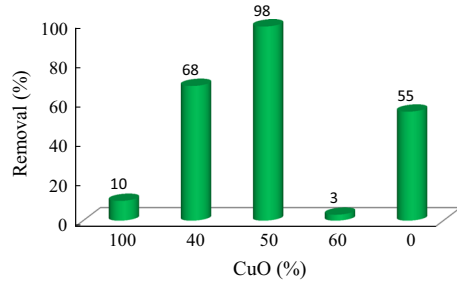


Fig. 9 The effect of the kind of adsorbent on the removal efficiency of MB



Adsorption kinetics

The pseudo-first order kinetic and pseudo-second order kinetic models were tested for examining the mechanism of adsorption.

A linear form of the pseudo-first order kinetic model [Eq. (2)] is given by:

$$\log(1 - q_t/q_e) = -k_1 t / 2.303 \quad (2)$$

where q_e , q_t and k_1 are the adsorbed MB at equilibrium (mg/g), the amount of the adsorbed MB at time t (mg/g) and the equilibrium rate constant of pseudo-first order kinetics (1/min), respectively.

The pseudo-second order kinetic model [Eq. (3)] is described by:

$$t/q_t = 1/k_2 q_e^2 + t/q_e \quad (3)$$

where k_2 is the equilibrium rate constant of the pseudo-second order model (g/mg min).

To understand the applicability of the above kinetics models, linear plots of $\log(1 - q_t/q_e)$ versus contact time (t), and t/q_t versus contact time (t) are plotted (Figs. 10, 11).

According to Fig. 11, the linear fit between the t/q_t versus contact time (t) and calculated R^2 for the pseudo-second order kinetics model show that the MB removal kinetics can be approximated as pseudo-second order kinetics.

Fig. 10 Linear fit of experimental data obtained using the pseudo-first order model ($m_{\text{ads}} = 0.01$ g, $C_0 = 10$ mg/L, $V = 10$ mL, natural pH, $T = \text{rt}$)

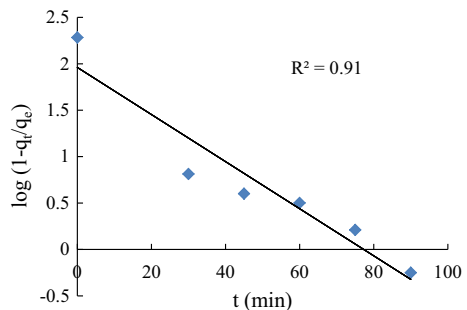
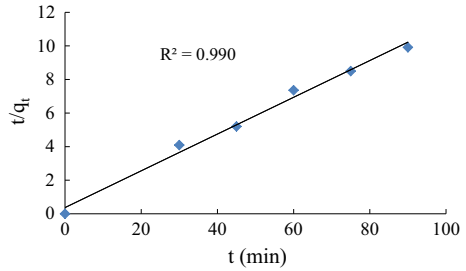


Fig. 11 Linear fit of experimental data obtained using the pseudo-second order model ($m_{ads} = 0.01$ g, $C_0 = 10$ mg/L, $V = 10$ mL, natural pH, $T = rt$)



Adsorption isotherms

The relation between the mass of the MB adsorbed onto adsorbent and liquid phase of the MB concentration can be investigated by the adsorption isotherm. In this study, the Langmuir [Eq. (4)] and Freundlich [Eq. (5)] isotherms were adopted to describe the adsorption behaviors of MB onto a nanocomposite.

The Langmuir isotherm is given as:

$$C_e/q_e = 1/q_{max}k_L + (1/q_{max})C_e \tag{4}$$

The Freundlich isotherm can be expressed by:

$$\log q_e = \log k_f + (1/n) \log C_e \tag{5}$$

Fig. 12 Linear fit of experimental data obtained using the Langmuir isotherm ($C_0 = 10$ mg/L, natural pH, $T = rt$)

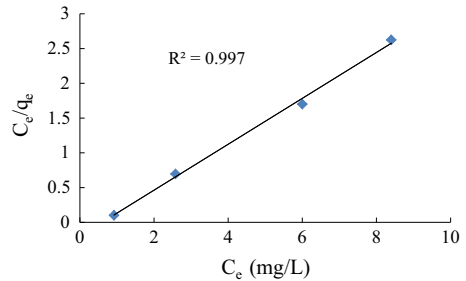
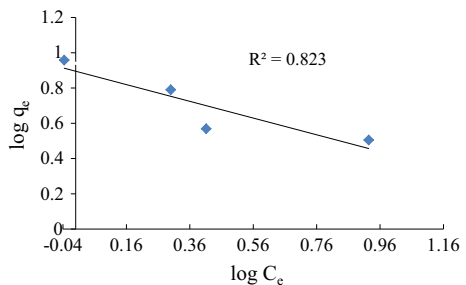


Fig. 13 Linear fit of experimental data obtained using the Freundlich isotherm ($b; C_0 = 10$ mg/L, natural pH, $T = rt$)



In the above equations, q_{\max} is the maximal sorption capacity at equilibrium (mg/g); k_L is the Langmuir constant related to the affinity of the binding sites and energy of adsorption (L/g); k_f is the Freundlich constant (L/mg), which indicates the relative adsorption capacity of the adsorbent; n is the heterogeneity factor and is known as the Freundlich coefficient. The linear plots of C_e/q_e versus C_e and $\log q_e$ versus $\log C_e$ are plotted in (Figs. 12, 13), respectively.

The R^2 values show that the MB removal isotherm using a nanocomposite follows the Langmuir isotherm.

Conclusion

Al₂O₃–SiO₂–CuO nanocomposites with different amounts of CuO (40, 50 and 60 %) were synthesized by the sol–gel method. These nanocomposites were used as adsorbents for the removal of methylene blue from aqueous solution. The nanocomposite with 50 % of CuO was chosen as an effective adsorbent. The optimum dosage and dye concentration were found to be 0.01 g and 10 mg/L, respectively. The kinetic data fit well with the pseudo-second order model according to the adsorption kinetics and the isotherm adsorption data fit well with the Langmuir model.

Acknowledgments We gratefully acknowledge financial support from the Research Council of the Islamic Azad University of Najafabad.

References

1. D.L. Lewis, A.W. Garrison, K.E. Wommack, A. Whittemore, P. Stuedler, J. Melillo, *Nature* **401**, 898 (1999)
2. S.A. Avlonitis, I. Poullos, D. Sotiriou, M. Pappas, K. Moutesidis, *Desalination* **221**, 259 (2008)
3. Q.Y. Yue, B.Y. Gao, Y. Wang, H. Zhang, X. Sun, S.G. Wang, R.R. Gu, *J. Hazard. Mater.* **152**, 221 (2008)
4. S. Wang, *Dyes Pigments* **76**, 714 (2008)
5. M. Sundrarajan, G. Vishnu, K. Joseph, *Dyes Pigments* **75**, 273 (2007)
6. J. Liu, S. Ma, L. Zang, *Appl. Surf. Sci.* **265**, 393 (2013)
7. H. Tajizadegan, M. Jafari, M. Rashidzadeh, A. Saffar-Teluri, *Appl. Surf. Sci.* **276**, 317 (2013)
8. W. Deligeer, Y.W. Gao, S. Asuha, *Appl. Surf. Sci.* **257**, 3524 (2011)
9. M. Anbia, S. Asl Hariri, S.N. Ashrafzadeh, *Appl. Surf. Sci.* **256**, 3228 (2010)
10. V.K. Gupta, R. Jain, A. Mittal, T.A. Saleh, A. Nayak, S. Agarwal, S. Sikarwar, *Mater. Sci. Eng. C* **32**, 12 (2012)
11. A. Mittal, J. Mittal, A. Malviya, D. Kaur, V.K. Gupta, *J. Colloid Interface Sci.* **342**, 518 (2010)
12. A. Mittal, D. Kaur, A. Malviya, J. Mittal, V.K. Gupta, *J. Colloid Interface Sci.* **337**, 345 (2009)
13. A. Mittal, J. Mittal, A. Malviya, V.K. Gupta, *J. Colloid Interface Sci.* **340**, 16 (2009)
14. V.K. Gupta, I. Ali, T.A. Saleh, A. Nayak, S. Agarwal, *RSC Adv.* **2**, 6380 (2012)
15. S. Karthikeyan, V.K. Gupta, R. Boopathy, A. Titus, G. Sekaran, *J. Mol. Liq.* **173**, 153–163 (2012)
16. A.K. Jain, V.K. Gupta, A. Bhatnagar, S. Suha, *Separ. Sci. Technol.* **38**, 463 (2003)
17. V.K. Gupta, I. Ali, *Water Res.* **35**, 33 (2001)
18. V.K. Gupta, S. Sharma, I.S. Yadav, D. Mohan, *J. Chem. Tech. Biotech.* **71**, 180 (1998)
19. T.A. Saleh, S. Agarwal, V.K. Gupta, *Appl. Catal. B: Environ.* **106**, 46 (2011)
20. V.K. Gupta, R. Kumar, A. Nayak, T.A. Saleh, M.A. Barakat, *Adv. Colloid Interface Sci.* **193**, 24 (2013)

21. V.K. Gupta, S.K. Srivastava, D. Mohan, S. Sharma, *Waste Manag.* **17**, 517 (1998)
22. V.K. Gupta, B. Gupta, A. Rastogi, S. Agarwal, A. Nayak, *Water Res.* **45**, 4047 (2011)
23. V.K. Gupta, A. Mittal, D. Jhare, J. Mittal, *RSC Adv.* **2**, 8381 (2012)
24. V.K. Gupta, I. Ali, V.K. Saini, T.V. Gerven, B.V. Bruggen, C. Vandecasteele, *Ind. Eng. Chem. Res.* **44**, 3655 (2005)
25. J.P. Chen, S. Wu, *Langmuir* **20**, 2233 (2004)
26. V. Vaccary, *Appl. Clay Sci.* **14**, 161 (1999)
27. M. Arshadi, M. Ghiaci, A. Gil, *Ind. Eng. Chem. Res.* **50**, 13628 (2011)
28. P.J. Sanchez-Soto, J.L. Perez-Rodríguez, I. Sobrados, J. Sanz, *J. Chem. Mater.* **9**, 677 (1997)
29. M. Arshadi, M. Ghiaci, A.A. Ensafi, H. Karimi-Maleh, S.L. Suib, *J. Mol. Catal. A: Chem.* **338**, 71 (2011)
30. A.A. Ensafi, H. Karimi-Maleh, M. Ghiaci, M. Arshadi, *J. Mater. Chem.* **21**, 15022 (2011)
31. M. Arshadi, M. Ghiaci, *Appl. Catal. A: Gen.* **399**, 75 (2011)
32. M. Arshadi, M. Ghiaci, A. Rahmanian, H. Ghaziaskar, A. Gil, *Appl. Catal. B: Environ.* **119**, 81 (2012)
33. Y. Ma, H. Li, R. Wang, H. Wang, W. Lv, S. Ji, *J. Power Sources* **289**, 22 (2015)
34. L. Li, L. Song, C. Chen, Y. Zhang, Y. Zhan, X. Lin, Q. Zheng, H. Wang, H. Ma, L. Ding, W. Zhu, *Int. J. Hydrog. Energ.* **39**, 19570 (2014)
35. M. Monte, D. Gamarra, A. LópezCámara, S.B. Rasmussen, N. Gyorffy, Z. Schay, A. Martínez-Arias, *J.C. Conesa, Catal. Today* **229**, 104 (2014)
36. L. Li, D. Mao, J. Yu, X. Guo, *J. Power Sources* **279**, 394 (2015)
37. P. Ling, D. Li, X. Wang, *J. Mol. Catal. A: Chem.* **357**, 112 (2012)
38. A. Ferdousi, J. Podder, J. Cry, *Process Technol.* **1**, 18 (2011)
39. M.J. Pattersona, D.E. Angovea, N.W. Canta, P.F. Nelsonb, *Appl. Catal. B: Environ.* **20**, 123 (1999)
40. A. Adamczyk, *J. Mol. Struct.* **614**, 127 (2002)
41. G.S. Machado, K.A.D.F. Castroa, O.J. Lima, E.J. Nassarb, K.J. Ciuffib, S. Nakagaki, *Colloid Surf. A. Physicochem. Eng. Asp.* **349**, 162 (2009)
42. J. Chandradass, B. Jun, D.S. Bae, *J. Noncryst. Solids* **354**, 3085 (2008)
43. M. Crisan, A. Jitianu, M. Zaharescu, F. Mizukami, S.I. Niwa, *J. Diser. Sci. Technol.* **24**, 13144 (2003)
44. M. Iranpour Mobarakeh, A. Saffar-Teluri, S.A. HassanzadehTabrizi, *Res. Chem. Intermed.* **41**, 6625 (2015)
45. K. Kadirvelu, C. Namasivayam, *Adv. Environ. Res.* **7**, 471 (2003)